Research article

Feng Liang, Degang Zhao*, Desheng Jiang, Wenjie Wang, Zongshun Liu, Jianjun Zhu, Ping Chen, Jing Yang and Liqun Zhang

Performance deterioration of GaN-based laser diode by V-pits in the upper waveguide layer

https://doi.org/10.1515/nanoph-2019-0449
Received October 30, 2019; revised December 2, 2019; accepted December 21, 2019

Abstract: The effect of V-pits in the upper waveguide (UWG) on device performance of GaN-based laser diodes (LDs) has been studied. Experimental results demonstrate that in comparison with the LDs with u-$In_{0.017}Ga_{0.983}N$/u-GaN multiple UWG or u-$In_{0.017}Ga_{0.983}N$ one, the LDs with a single u-GaN UWG has the best device performance. They have a smaller threshold current density, and a larger and more stable output optical power. The lowest threshold current density is as low as 1.3 kA/cm^2, and the optical power reaches to 2.77 W. Furthermore, atomic force microscopy suggests that the deterioration of device performance of former kinds of devices may be attributed to the increase of V-pits' size and quantity in the undoped-$In_{0.017}Ga_{0.983}N$ UWG layer, and these V-pits could introduce more nonradiative recombination centers and exacerbate the inhomogeneity of injection current. Moreover, theoretical calculation results indicate that the increase of leakage current and optical loss are additional reasons for the device performance deterioration, which may be caused by a reduction of the potential barrier height for electrons in the quantum wells and by an increased background electron concentration in UWG.

Keywords: GaN-based laser diode; V-pits; upper waveguide layer.

OCIS codes: (140.5960) Semiconductor lasers; (230.7370) Waveguides.

1 Introduction

GaN-based laser diodes (LDs) have important application prospects in car headlights, general lighting, atomic clocks, portable projection, laser-based TVs, underwater communication, quantum technology and high-density optical data storage [1–11]. A great progress has been made in the last 30 years since Nakamura demonstrated the first GaN-based blue-violet diode lasers in 1990 [12, 13]. The upper waveguide (UWG) is significant for blue and green GaN-based LDs to confine the optical field, and many works focus on a comparative analysis between a p-type (In)GaN UWG layer and an undoped (In)GaN UWG layer [14–17]. Actually, during epitaxial growth of LDs with the metal organic chemical vapor deposition, a high density of defects like V-pits in InGaN would be formed due to the phase separation and inhomogeneity of indium caused by the poor impermissibility between GaN and InN [18–20]. Meanwhile, the defect density would increase along with the increases of thickness or indium content of InGaN waveguide layer. However, less attention is put forward to build a connection between the V-pits in UWG layer and the device performance of GaN-based LD, although extensive works have focused on the V-pits' structural feature, formation mechanism [21–23] and influence on the performance of light-emitting diodes [24, 25] and solar cells [26, 27]. Therefore, GaN-based LDs with different (In)GaN UWG layer have been investigated in this study experimentally and theoretically. Experimental results demonstrate that the performance deterioration of the

***Corresponding author: Degang Zhao,** State Key Laboratory of Integrated Optoelectronics, Institute of Semiconductors, Chinese Academy of Sciences, Beijing 100083, China; and Center of Materials Science and Optoelectronics Engineering, University of Chinese Academy of Sciences, Beijing 100049, China, e-mail: dgzhao@red.semi.ac.cn
Feng Liang, Desheng Jiang, Zongshun Liu, Ping Chen and Jing Yang: State Key Laboratory of Integrated Optoelectronics, Institute of Semiconductors, Chinese Academy of Sciences, Beijing 100083, China. https://orcid.org/0000-0002-2064-8918 (F. Liang)
Wenjie Wang: Microsystem and Terahertz Research Center, Chinese Academy of Engineering Physics, Chengdu 610200, China
Jianjun Zhu: State Key Laboratory of Integrated Optoelectronics, Institute of Semiconductors, Chinese Academy of Sciences, Beijing 100083, China; and Center of Materials Science and Optoelectronics Engineering, University of Chinese Academy of Sciences, Beijing 100049, China
Liqun Zhang: Suzhou Institute of Nano-tech and Nano-bionics, Chinese Academy of Sciences, Suzhou 215123, China

GaN-based blue-violet LDs would be related to the V-pits in the UWG layer, and an increase of leakage current and optical loss is another reason according to the theoretical calculation result by LASTIP.

2 Fabrication and theoretical calculation of GaN-based LDs

Three GaN-based blue-violet LDs with different UWG layers are fabricated, i.e. LDI, LDII and LDIII, which are grown in an AIXTRON 3×2 in. close-coupled showerhead reactor on c-plane GaN substrates. The schematic structure of LDI, LDII and LDIII is shown in Figure 1. A thick n-GaN layer is grown on GaN substrate firstly, and then a n-type cladding layer (CL), a lower waveguide layer, a multiple quantum well active region, an UWG layer, an electron blocking layer, a p-type CL and a heavily Mg-doped GaN (p^{++}-GaN) contact layer are grown successively. During growth, TMGa/TEGa, TMAl, TMIn, NH_3, Cp_2Mg and SiH_4 are used as Ga, Al, In, N, Mg and Si sources, respectively. Between LDI, LDII and LDIII, only the UWG is different. The UWG in LDI and LDIII is a 93-nm unintentionally doped-GaN layer (u-GaN) and a 93-nm unintentionally doped-$In_{0.017}Ga_{0.983}N$ layer (u-$In_{0.017}Ga_{0.983}N$), respectively. For LDII, the UWG consists of a 50-nm u-GaN layer and a 43-nm u-$In_{0.017}Ga_{0.983}N$ layer. A 15-μm-wide ridge stripe was formed by dry etching along the <1–100> direction, and a 1200-μm-long cavity was fabricated by cleaving along the {1–100} plane. Then the front and rear cleaved cavity facets are coated to get a reflectivity of 10% and 90%, respectively. As a part of a vertical LD structure, the Ti/Pt/Au and Pd/Pt/Au are used as n-type and p-type metal electrodes, respectively.

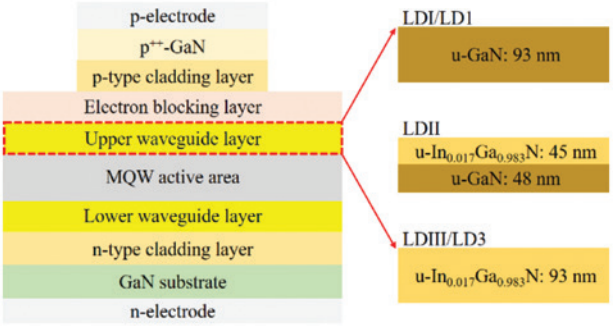

Figure 1: The schematic structure of the GaN-based LDs with different upper waveguide.

Moreover, a 93-nm-thick u-GaN layer and a 93-nm-thick InGaN layer are prepared as reference samples for investigating surface quality of the layers. They are grown separately on sapphire substrate and under the same conditions as u-GaN and InGaN waveguide layers in LDI and LDIII. As schematically shown in Figure 2A, the reference sample structure is a thin unintentionally doped GaN nucleation layer (LT-GaN), a 2-μm-thick high-temperature grown GaN template (u-GaN) and a top u-InGaN layer. The 93-nm-thick InGaN layer is also used to check the thickness and indium content of the grown layer by X-ray diffraction (XRD). A ω-2θ XRD rocking curve at (002) reflection of this u-InGaN waveguide layer is shown in Figure 2B. It can be seen that there are two diffraction peaks in the high resolution (002) ω-2θ XRD rocking curves near 34.5°, and

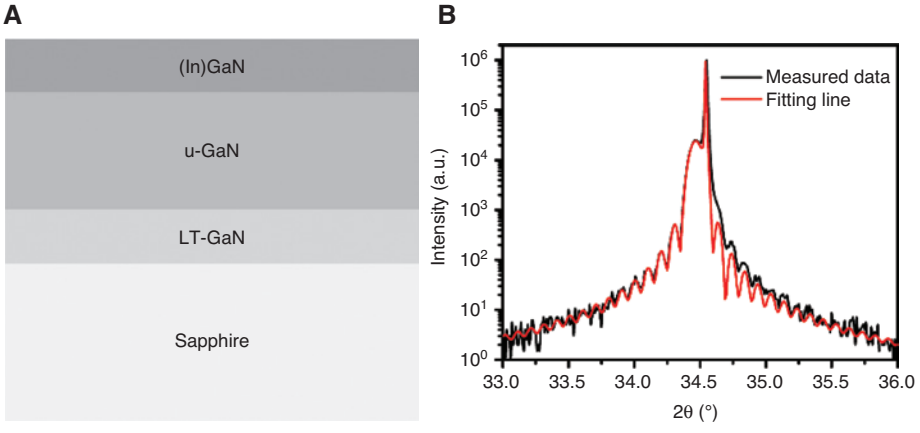

Figure 2: As schematically shown in (A), the reference sample structure is a thin unintentionally-doped GaN nucleation layer (LT-GaN), a 2 μm-thick high-temperature grown GaN template (u-GaN) and a top u-InGaN layer. (B) Gives the ω-2θ X-ray diffraction (XRD) rocking curves at (002) reflection of the u-InGaN waveguide layer, and the diffraction peaks located in the low and high angles of 2θ are originated from the InGaN and GaN layers, respectively.
(A) The schematic diagram of device stack with a top u-InGaN layer and (B) the (002) ω-2θ rocking curves of u-InGaN layer.

other diffraction peaks located in the low and high angles of 2θ originate from the InGaN and GaN layers, respectively. According to the fitting result, the indium content and thickness of this u-InGaN layer are around 1.7% and 93 nm, respectively.

In addition, two GaN-based blue-violet LDs, i.e. LD1 and LD3, are studied theoretically with LASTIP program (Crosslight Software Inc.). LASTIP is a powerful software for calculating and analyzing the optical and electrical characteristics of LD thermionically by self-consistently solving the Poisson's equations and the current continuity equations [28, 29]. In fact, LD1 and LD3 are designed based on the structures of LDI and LDIII, respectively. It means that only the UWG layer is different between LD1 and LD3. The UWG layer in LD1 and LD3 is a 93-nm u-GaN layer and a 93-nm u-$In_{0.017}Ga_{0.983}N$ layer, respectively. The thickness and doping level of each layer in these two LD structures are listed in Table 1. Moreover, the cavity length of LD1 and LD3 is set to be 600 μm, and the stimulated wavelength is around 405 nm. In addition, the screening factor in LASTIP calculation is set to be 25%, which means 25% of the theoretical interface charge is taken during calculation [30, 31]. As shown in Figure 3, the refractive indexes of AlGaN and InGaN alloys are estimated in a way similar to what proposed by Laws et al. [32] and Piprek et al. [33, 34].

Table 1: Structural parameters of LD1 and LD3 for calculation with LASTIP.

Layer	Thickness	Doping (cm^{-3})
n-GaN substrate	1 μm	3×10^{18}
n-$Al_{0.08}Ga_{0.92}N$ CL	1 μm	3×10^{18}
n-GaN LWG	120 nm	5×10^{17}
MQW	$In_{0.11}Ga_{0.89}N$ Well: 6.0 nm	QW: 1×10^{16}
	GaN Barrier: 15 nm	QW: 5×10^{17}
UWG	LD1: 93 nm u-GaN	1×10^{17}
	LD3: 93 nm $In_{0.017}Ga_{0.983}N$	
p-$Al_{0.15}Ga_{0.85}N$ EBL	20 nm	5×10^{19}
p-$Al_{0.06}Ga_{0.94}N$ CL	600 nm	2×10^{19}
Contact layer	40 nm	1×10^{20}

3 Results and discussion

3.1 Experimental results

Figure 4 shows the optical power of three prepared GaN-based blue-violet LD devices as a function of the forward direct current and the optical spectrum of stimulated emission. It can be seen that the peak wavelength of the optical spectrum is around 404.5 nm, and the full width at half maximum of this peak is small. In addition, the threshold current of LDI, LDII and LDIII is around 220.0 mA, 298.1 mA and 555.2 mA, respectively, and the corresponding threshold current density is about 1.2 kA/cm², 1.7 kA/cm² and 3.1 kA/cm², respectively. The peak optical power of LDI, LDII and LDIII is about 2.77 W, 1.81 W and 0.72 W, respectively, at a corresponding current around 3.0 A, 1.92 A and 1.65 A, respectively. It is noted that except for LDI, the optical power of LDII and LDIII increases first and then decreases abruptly when the current increases up to 3 A. It means that the device performance of LDI is the best among the three LDs, i.e. having the lowest threshold current, the largest peak optical power and the most

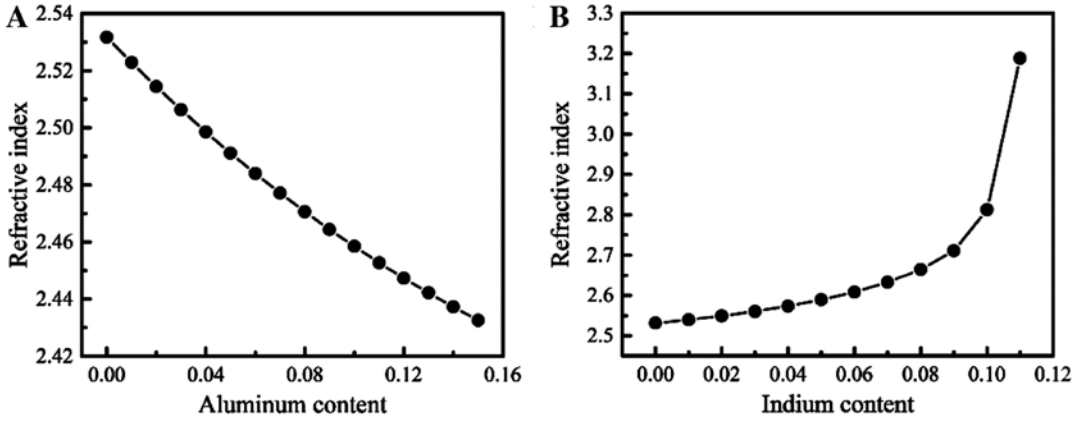

Figure 3: The refractive indexes of AlGaN decrease along with the aluminum increasing, and the refractive indexes of InGaN alloys increase along with the indium increasing.
Estimated refractive indexes of AlGaN (A) and InGaN (B) alloys during calculation.

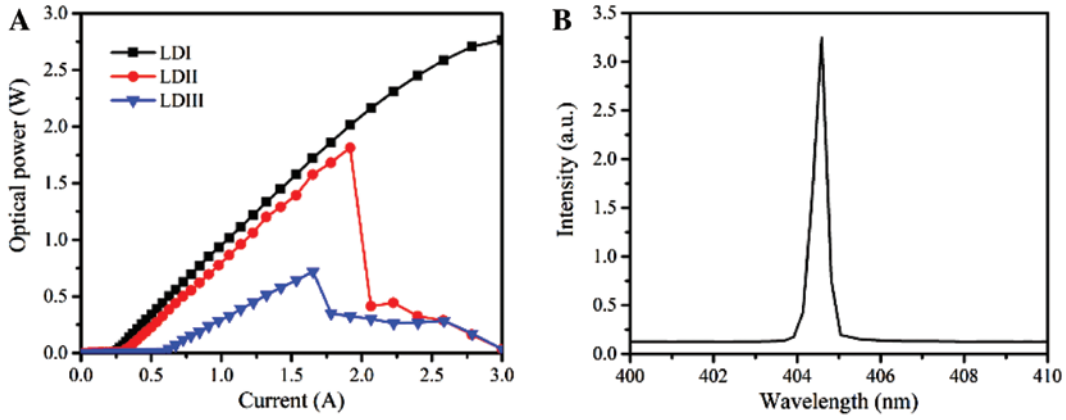

Figure 4: (A) Shows the optical power of 3 prepared GaN-based blue-violet LD devices as a function of the forward direct-current and (B) gives the optical spectrum of stimulated emission. The threshold current of LDI, LDII and LDIII is around 220.0 mA, 298.1 mA and 555.2 mA, respectively, and the peak optical power of LDI, LDII and LDIII is about 2.77 W, 1.81 W and 0.72 W, respectively.
(A) Optical power vs. current (*P-I*) curves of the LDI (black). LDII (red) and LDIII (blue), and (B) The optical spectrum of stimulated emission measured at room temperature.

stable output. This experimental result demonstrates that the device performance could be weakened when using the u-GaN/u-$In_{0.017}Ga_{0.983}N$ multiple UWG layer or using a u-$In_{0.017}Ga_{0.983}N$ UWG layer.

To find the reason for the weaker performance of LDII and LDIII, the atomic force microscopy (AFM) measurements are taken to check the surface topography of the 93-nm-thick u-GaN and u-InGaN layer reference samples. Figure 5A and B show that in a 5 μm × 5 μm region, the root-mean-square roughness of the 93-nm-thick u-GaN layer and the 93-nm-thick u-$In_{0.017}Ga_{0.983}N$ layer is 0.54 nm and 2.06 nm, respectively, which means that the surface of the u-$In_{0.017}Ga_{0.983}N$ layer is much coarser. It is also noted that V-pits are formed in both u-GaN and u-$In_{0.017}Ga_{0.983}N$, but the size of V-pits in the u-$In_{0.017}Ga_{0.983}N$ layer is clearly much bigger than that in the u-GaN layer. Meanwhile, the quantity of V-pits in the u-$In_{0.017}Ga_{0.983}N$ layer is also much larger than that in the u-GaN layer. The V-pit density of u-GaN and u-$In_{0.017}Ga_{0.983}N$ is estimated to be 1 μm^{-2} and 6 μm^{-2}, respectively, in a 5 μm × 5 μm region; i.e. the V-pit density of the 93-nm-thick u-GaN layer is about 6 times smaller than that of the 93-nm-thick u-$In_{0.017}Ga_{0.983}N$ layer. In addition, Figure 5C shows the distribution of the V-pit's depth. It indicates that the depth of most V-pits in u-GaN and u-$In_{0.017}Ga_{0.983}N$ is about 1.8 nm and 3.6 nm, respectively. Meanwhile, very few V-pits have a depth larger than 4 nm in the u-GaN layer, but the V-pit depth in the u-$In_{0.017}Ga_{0.983}N$ layer can reach up to 6 nm. This result demonstrates that the average depth and density of V-pits in the 93-nm-thick u-$In_{0.017}Ga_{0.983}N$ layer are much larger than that in the 93-nm-thick u-GaN layer, indicating that the material quality of the u-GaN layer is much better than the u-$In_{0.017}Ga_{0.983}N$ layer.

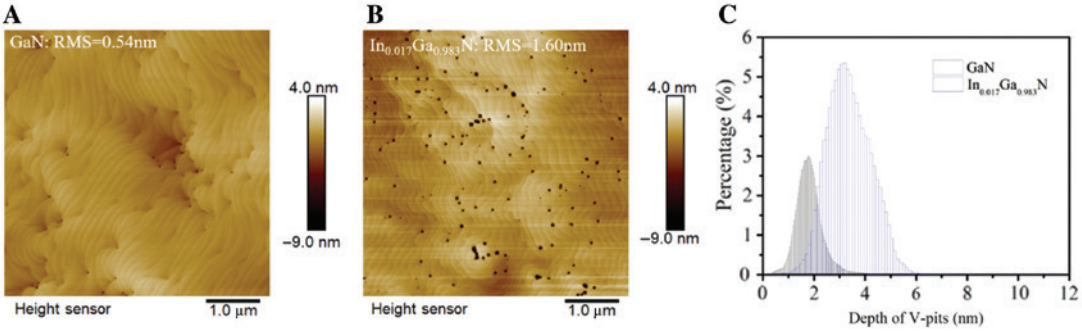

Figure 5: The root-mean-square (RMS) roughness of the 93 nm-thick u-GaN layer and the 93 nm-thick u-$In_{0.017}Ga_{0.983}N$ layer is 0.54 nm and 2.06 nm, respectively, and the size and quantity of V-pits in u-$In_{0.017}Ga_{0.983}N$ layer is clearly much bigger than those in u-GaN layer. In addition, the average depth and density of V-pits in the 93 nm-thick u-$In_{0.017}Ga_{0.983}N$ layer are much larger than that in the 93 nm-thick u-GaN layer. Atomic force microscopy images for (A) 93-nm-thick u-GaN and (B) 93-nm-thick u-In0.017Ga0.983N layers, and (C) the distribution of V-pit depth (blue for InGaN surface and black for GaN one).

It is known that V-defects originate from the InGaN layers intercepted by threading dislocations. V-defects may preferentially capture carriers, subsequently enhance local current and influence the local carrier recombination. Some reported investigations show that V-pits have positive effects like enhancing the extraction of the photogenerated carriers in the InGaN absorber or enhanced output power of InGaN light emitting diode [24, 26]. However, there are also other reports which show that V-pits can have negative effects such as increasing leakage current and reducing emission efficiency of InGaN-based light-emitting diodes [23]. In this study, the obtained result suggests that the higher threshold current density and lower optical power of LDIII and LDII are deteriorated, and they may be related to the denser and larger V-pits in their UWG layers.

Furthermore, conductive AFM (c-AFM) measurement is employed to obtain the distribution of forward current on the u-$In_{0.017}Ga_{0.983}N$ layers and to check the carrier injection around the V-pits. It should be able to give a clue to find the reason for the unstable output optical power of LDII and LDIII. Figure 6 shows the c-AFM current images which is measured at a 2.0 V bias in the same region as shown in Figure 5B. It is noted that in forward bias condition an enhanced current occurs around the V-pits area. Actually, our previous work has demonstrated that V-pits could result in a larger reverse-bias leakage current and a lower electroluminescence in the studied InGaN-based light-emitting diodes, in which the V-pits are originated from the InGaN well layer [23]. It suggests that the unstable output optical power of LDII and LDIII may be related to the inhomogeneity of carrier injection around the V-pits. This inhomogeneity could be aggravated when the density and size of V-pits in the UWG layer increase. It even may result in an abrupt rise of leakage current at higher injection current, as what we have observed in the optical power curves of LDII and LDIII. Therefore, based on the observed difference in the V-pits, it can well explain why LDIII performs worse than LDI in the stability of output optical power.

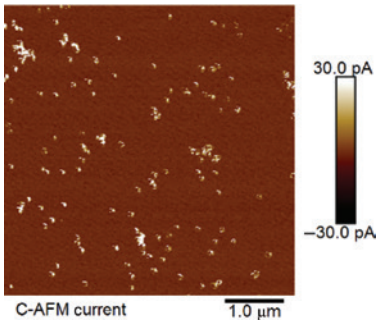

Figure 6: Conductive atomic force current image at 2.0 V of 93-nm-thick u-$In_{0.017}Ga_{0.983}N$ layer reference sample.

3.2 Theoretical results

To check whether there are other factors influencing the device performance in addition to the V-pits in the waveguide layer, the performances of two LDs, i.e. LD1 and LD3, are calculated through LASTIP simulation. The structure parameters of LD1 and LD3 are shown in Table 1, and no influence of V-pits is considered during the theoretical calculation. During calculation, the absorption coefficient of each layer is simply set to be proportional to its doping concentration in a way similar to that proposed by Huang et al. [35], i.e.

$$\text{Absorption coefficient} = \frac{\text{doping level } (\text{cm}^{-3})}{10^{19}\ (\text{cm}^{-3})} \times 50\ (\text{cm}^{-3}) \tag{1}$$

It means that the absorption coefficient of u-GaN and u-$In_{0.017}Ga_{0.983}N$ UWG layer is the same, i.e. 2.5 cm^{-1} cm.

The optical field distribution is checked first. Figure 7A shows that the optical field is moved towards the p-side slightly when using a u-$In_{0.017}Ga_{0.983}N$ UWG layer. The calculated result shows that the optical confinement factor of LD1 and LD3 is 0.58% and 6.13%, respectively. It means that using a u-$In_{0.017}Ga_{0.983}N$ UWG layer can improve the optical field distribution. Moreover, the calculated output optical power vs. current (*P-I*) of LD1 and LD3 is shown in Figure 7B. It can be seen from Figure 7B that the threshold current of LD1 and LD3 is 27.1 mA, and 36.6 mA, respectively. Meanwhile, at the same injection current of 120 mA, the output optical power of LD1 and LD3 is 115.6 mW and 72.1 mW, respectively. It is clear that the device performance of LD3 is not as good as LD1. This result demonstrates that using a u-$In_{0.017}Ga_{0.983}N$ UWG layer would weaken the device performances remarkably compared to a u-GaN UWG layer when the absorption coefficients of the u-$In_{0.017}Ga_{0.983}N$ and u-GaN layers are set to be the same. This result suggests that when the UWG layer material is changed, there are indeed other factors that can also have influence on the device performance in addition to the V-pits. Thus, the difference of electron current density and conduction band should be discussed below in detail.

Figure 8A shows the vertical electron current density distribution surrounding the active region along the growth direction at an injection current of 120 mA. Electrons are injected from the n-type side and then recombined with

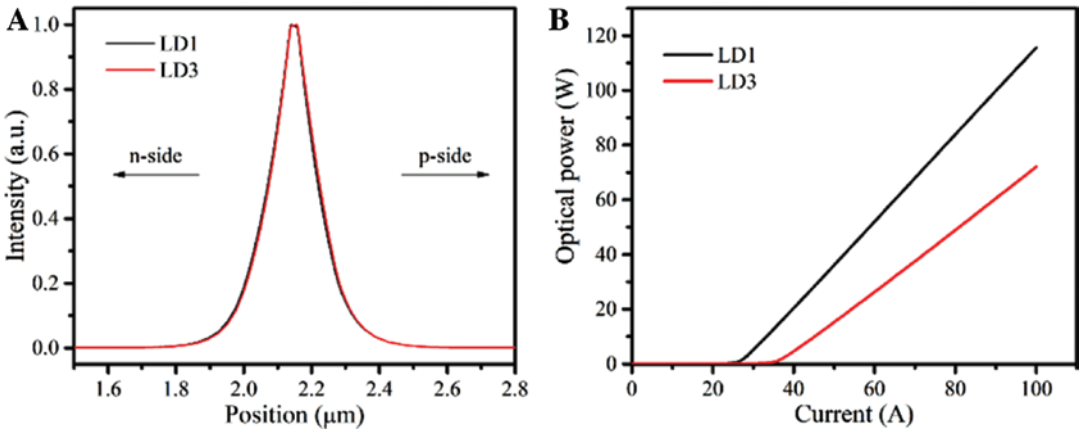

Figure 7: The optical field is moved towards the p-side slightly when using a u-$In_{0.017}Ga_{0.983}N$ upper waveguide layer. Moreover, the threshold current of LD1 and LD3 is 27.1 mA, and 36.6 mA, respectively, and the output optical power of LD1 and LD3 is 115.6 mW and 72.1 mW, respectively, at the same injection current of 120 mA.
(A) Optical field distribution and (B) optical power vs. current of the LD1 (black) and LD3 (red).

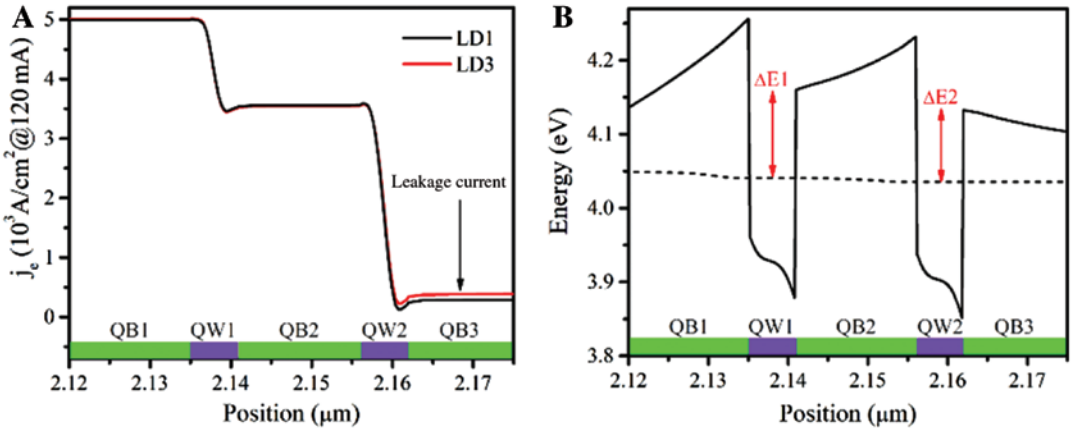

Figure 8: Shows the vertical electron current density distribution around the active region along the growth direction at an injecting current of 120 mA and the conduction band diagram. It can be seen that the leakage current of LD3 is larger than that of LD1, and the effective barrier height for the electrons in LD3 is smaller than that of LD1.
Vertical electron current density distribution around the active region along the growth direction for LD1 (black) and LD3 (red) at an injecting current of 120 mA (A), and the conduction band diagrams (B). The short dot marks the quasi-Fermi levels of electron.

the holes in the active region, which results in a reduction of electron current density around the first quantum well (QW1) and the second quantum well (QW2). Moreover, the leakage current can be defined as the current going out from the last quantum barrier (QB3), which is marked with the black arrows in Figure 8A. It is noted that the leakage current of LD3 is larger than that of LD1. This result provides an evidence that an increase of leakage current is perhaps another reason for the performance deterioration of LD3 in addition to the leakage induced by the V-pits in waveguide layer. Moreover, the reason for the increase of leakage current in LD3 can also be analyzed by examining the change of conduction band in LD1 and LD3. Figure 8B gives the conduction band diagram under an injection current of 120 mA, in which the electron barrier height in quantum well is marked with the double-headed arrow. The electron barrier height is defined as the energy differences between the electron quasi-Fermi level in quantum well and quantum barrier, i.e. ΔE1 and ΔE2, which can be used to reflect the effective blocking ability of the second barrier (QB2) and the last barrier (QB3) for the electrons. For LD1, ΔE1 and ΔE2 are 120 meV and 98 meV, respectively. For LD3, ΔE1 and ΔE2 are 111 meV and 90 meV, respectively. It means that the effective barrier height for the electrons in LD3 is smaller than that of LD1. That is why the leakage current in LD3 is larger than that of

LD1, and the parameters of the threshold current and the output light power of LD3 are poorer than those of LD1. This result suggests that reduction of the energy barrier height for electrons should be the other reason for the device performance deterioration of LDII and LDIII.

In addition, it is noted that the change of UWG material may have influence on the background carrier concentration of the UWG. Therefore, Hall measurement is taken to obtain the background electron concentration using van der Pauw method at 300 K for both u-$In_{0.017}Ga_{0.983}N$ and u-GaN waveguide layers. Hall measurement result shows that the background electron concentration of the u-$In_{0.017}Ga_{0.983}N$ and u-GaN single layer is 4.4×10^{17} cm^{-3} and 1.4×10^{16} cm^{-3}, respectively. This differencemight be caused by the density difference of point defects in u-$In_{0.017}Ga_{0.983}N$ and u-GaN, such as gallium vacancies (V_{Ga}), nitrogen vacancies (V_{Ga}) and their complexes. Thus, in addition to LD3, the performance of another LD, named LD3-1, is also calculated, and the absorption coefficient of the u-$In_{0.017}Ga_{0.983}N$ waveguide layer in LD3-1 is set to be 750 cm^{-1} instead of 2.5 cm^{-1}. The calculated result shows that the optical loss of LD1, LD3 and LD3-1 is 21.5 cm^{-1}, 39.5 cm^{-1}, 44.9 cm^{-1}, respectively. Meanwhile, the threshold current and optical power at 120 mA of LD3-1 is about 42.1 mA and 68.0 mW, respectively. It indicates that a higher background electron concentration of the u-$In_{0.017}Ga_{0.983}N$ waveguide layer could also result in a deterioration of device performance. These results suggest that, except for the influence of V-defects, the reduced barrier height and a higher background electron concentration of the u-$In_{0.017}Ga_{0.983}N$ waveguide layer might be an additional reason for the deterioration of LDIII.

4 Summary

The influence of the UWG layer has been studied experimentally and theoretically. The device performance deterioration with the u-$In_{0.017}Ga_{0.983}N$ waveguide layer is attributed to the increase of leakage current caused by the increase of V-pits' size and quantity. The increase of leakage current is due to the reduction of the energy barrier height for the electrons in quantum wells, and the increase of optical loss is caused by the higher background electron concentration. They may be additional reasons for the deterioration of the device performance. Moreover, c-AFM analysis result shows that the unstable optical power of LDs using the u-$In_{0.017}Ga_{0.983}N$ UWG layer can be attributed to the inhomogeneous injection current around the V-pits.

Funding: The authors acknowledge the support from Science Challenge Project (Grant No. TZ2016003), National Key R&D Program of China (Grant Nos. 2018YFB0406903, 2016YFB0401801 and 2016YFB0401803), and National Natural Science Foundation of China (Grant Nos. 61674138, 61674139, 61604145, 61574135, and 61574134).

Disclosures: The authors declare that there are no conflicts of interest related to this article.

References

[1] Hardy MT, Feezell DF, DenBaars SP, Nakamura S. Group III-nitride lasers: a materials perspective. Mater Today 2011;14:408–15.

[2] Alahyarizadeh G, Amirhoseiny M. Performance characteristics of deep violet InGaN DQW lasers based on different compliance layers. Optik 2017;131:194–200.

[3] Zhao DG, Jiang DS, Le LC, et al. Performance improvement of GaN-based violet laser diodes. Chinese Phys Lett 2017;34:017101.

[4] Kim J, Kim H, Lee SN. Thermal degradation in InGaN quantum wells in violet and blue GaN-based laser diodes. Curr Appl Phys 2011;11:S167–70.

[5] Masui S, Nakatsu Y, Kasahara D, Nagahama S. Recent improvement in nitride lasers. in *SPIE Gallium Nitride Materials and Devices XII* 2017;10104:101041H. Available at: https://doi.org/10.1117/12.2247988.

[6] Moustakas TD, Paiella R. Optoelectronic device physics and technology of nitride semiconductors from the UV to the terahertz. Rep Prog Phys 2017;80:106501.

[7] Goldberg GR, Ivanov P, Ozaki N, et al. Gallium nitride light sources for optical coherence tomography. in *SPIE Gallium Nitride Materials and Devices XII* 2017;10104:101041X. Available at: https://doi.org/10.1117/12.2252665.

[8] Ali M, Gerhard S, Stojetz B, et al. High-power diode lasers and their applications. in *Laser Processing of Materials and Industrial Applications II* 1998;3550:450. Available at: https://doi.org/10.1117/12.317956.

[9] Kneissl M, Rass J. III-Nitride ultraviolet emitters. Cham, Switzerland, Springer International Publishing, 2016. Available at: https://doi.org/10.1007/978-3-319-24100-5.

[10] Yang J, Zhao DG, Liu ZS, et al. Fabrication of room temperature continuous-wave operation GaN-based ultraviolet laser diodes. J Semicond 2017;38:051001.

[11] Jiang LJ, Tian AQ, Cheng Y, et al. GaN-based green laser diodes. J Semicond 2016;37:111001.

[12] Shuji N, Masayuki S, Shin-ichi N, et al. Violet InGaN/GaN/AlGaN-based laser diodes with an output power of 420 mW. Jan J Appl Phys 1998;37:L627.

[13] Shuji N, Masayuki S, Shin-ichi N, et al. InGaN-based multi-quantum-well-structure laser diodes. Jan J Appl Phys 1996;35:L74.

[14] Liang F, Yang J, Zhao DG, et al. Room-temperature continuous-wave operation of GaN-based blue-violet laser diodes with a lifetime longer than 1000 h. J Semicond 2019;40:022801.

[15] Liang F, Zhao DG, Jiang DS, et al. Performance enhancement of the GaN-based laser diode by using an unintentionally doped GaN upper waveguide. Jan J Appl Phys 2018;57:070307.

[16] Zhang LQ, Jiang DS, Zhu JJ, et al. Confinement factor and absorption loss of AlInGaN based laser diodes emitting from ultraviolet to green. J Appl Phys 2009;105:023104.
[17] Alahyarizadeh G, Amirhoseiny M, Hassan Z. Effect of different EBL structures on deep violet InGaN laser diodes performance. Opt Laser Technol 2016;76:106–12.
[18] Wang H, Jiang DS, Jahn U, et al. Investigation on the strain relaxation of InGaN layer and its effects on the InGaN structural and optical properties. Physica B: Condensed Matter 2010;405:4668–72.
[19] Osamura K, Naka S, Murakami Y. Preparation and optical properties of $Ga_{1-x}In_xN$ thin films. J Appl Phys 1975;46:3432–7.
[20] Ponce FA, Srinivasan S, Bell A, Geng L, Tanaka S. Microstructure and electronic properties of InGaN alloys. Phys Stat Sol B 2003;240:273–84.
[21] Chen Y, Takeuchi T, Amano H, et al. Pit formation in GaInN quantum wells. Appl Phys Lett 1998;72:710–2.
[22] Kim IH, Park HS, Park YJ, Kim T. Formation of V-shaped pits in InGaN/GaN multiquantum wells and bulk InGaN films. Appl Phys Lett 1998;73:1634–6.
[23] Le LC, Zhao DG, Jiang DS, et al. Carriers capturing of V-defect and its effect on leakage current and electroluminescence in InGaN-based light-emitting diodes. Appl Phys Lett 2012;101:252110.
[24] Han D, Ma S, Jia Z, et al. Photoluminescence close to V-shaped pits in the quantum wells and enhanced output power for InGaN light emitting diode. J Phys D Appl Phys 2017;50:475103.
[25] Kim DH, Park YS, Kang D, Kim K-K, Seong TY, Amano H. Combined effects of V pits and chip size on the electrical and optical properties of green InGaN-based light-emitting diodes. J Alloy Compd 2019;796:146–52.
[26] Arif M, Salvestrini JP, Streque J, et al. Role of V-pits in the performance improvement of InGaN solar cells. Appl Phys Lett 2016;109:133507.
[27] Cai XM, Zheng ZW, Long H, Ying LY, Zhang BP. Abnormal staircase-like I-V curve in InGaN quantum well solar cells. Appl Phys Lett 2018;112:161102.
[28] Li X, Zhao DG, Jiang DS, et al. Fabrication of ridge waveguide of 808 nm GaAs-based laser diodes by wet chemical etching. J Semicond 2015;36:074009.
[29] Pang Y, Li X, Zhao B. Influence of the thickness change of the wave-guide layers on the threshold current of GaAs-based laser diode. J Semicond 2016;37:084007.
[30] Fiorentini V, Bernardini F, Ambacher O. Evidence for nonlinear macroscopic polarization in III–V nitride alloy heterostructures. Appl Phys Lett 2002;80:1204–6.
[31] Bernardini F, Fiorentini V. Nonlinear macroscopic polarization in III-V nitride alloys. Phys Rev B 2001;64:085207.
[32] Laws GM, Larkins EC, Harrison I, Molloy C, Somerford D. Improved refractive index formulas for the $Al_xGa_{1-x}N$ and $In_yGa_{1-y}N$ alloys. J Appl Phys 2001;89:1108–15.
[33] Piprek J, Peng T, Qui G, Olowolafe JO. Energy gap bowing and refractive index spectrum of AlInN and AlGaInN. In: *Compound Semiconductors 1997. Proceedings of the IEEE Twenty-Fourth International Symposium on Compound Semiconductors,* San Diego, CA, USA, 1997:227–30. Available at: https://ieeexplore.ieee.org/document/711623.
[34] Peng T, Piprek J. Refractive index of AlGaInN alloys. Electron Lett 1996;32:2285–6.
[35] Huang CY, Lin YD, Tyagi A, et al. Optical waveguide simulations for the optimization of InGaN-based green laser diodes. J Appl Phys 2010;107:023101.